LONGITUDINAL GROWTH MODELING OF DISCRETE-TIME FUNCTIONS WITH APPLICATION TO DTI TRACT EVOLUTION IN EARLY NEURODEVELOPMENT

Anuja Sharma[1] *Stanley Durrleman*[2] *John H. Gilmore*[3] *Guido Gerig*[1] *

[1]School of Computing, SCI Institute, University of Utah, Salt Lake City, UT 84112, USA
[2]INRIA-Asclepios project, 2004 route des Lucioles, 06902 Sophia Antipolis, France
[3] UNC Chapel Hill, Department of Psychiatry, Chapel Hill, NC 27599-7160, USA

ABSTRACT

We present a new framework for spatiotemporal analysis of parameterized functions attributed by properties of 4D longitudinal image data. Our driving application is the measurement of temporal change in white matter diffusivity of fiber tracts. A smooth temporal modeling of change from a discrete-time set of functions is obtained with an extension of the logistic growth model to time-dependent spline functions, capturing growth with only a few descriptive parameters. An unbiased template baseline function is also jointly estimated. Solution is demonstrated via energy minimization with an extension to simultaneous modeling of trajectories for multiple subjects. The new framework is validated with synthetic data and applied to longitudinal DTI from 15 infants. Interpretation of estimated model growth parameters is facilitated by visualization in the original coordinate space of fiber tracts.

Index Terms— spatiotemporal modeling, growth functions, longitudinal image data, diffusion tensor imaging, early brain development

1. INTRODUCTION

Medical imaging has been gaining increasing importance due to its potential to study dynamic anatomical and physiological changes invivo. Longitudinal imaging yields improved understanding of average, representative growth trends in healthy individuals along with their natural variability. This knowledge is critical to clinical research as a systematic comparison of individual trends to the average scenario can lead to timely diagnosis and prognosis of diseases. In this paper, we develop methods to study temporal changes in individuals and populations with application to human brain development.

Many authors have contributed to the understanding of neurodevelopment, for instance, changes with time in morphometric measures like brain shape and white matter maturation [1, 2, 3, 4]. However, the cross-sectional design employed in these analyses compares data at specific time points. Therefore, such methods pose severe limitations while dealing with longitudinal data as they do not account for the correlation between repeated scans. In contrast, a longitudinal design utilizes the complete temporal change information of individuals and hence is better suited for analyzing serial data, specially if the inter-subject cross sectional variability is more dominant than the temporal trend [5]. Recent work addresses longitudinal modeling in MRI [6, 7, 8]. However, most of these explore the 'average' change over time for the population but in the process, fail to capture an individual's growth independently. Without characterizing patient-specific patterns for comparison with normative trajectories, designing and administering individualized medical treatments may not be optimal [5]. This is one of the key limitations we address in this paper. Additionally, many existing longitudinal analysis frameworks rely on curve-fitting to cumulative volume measures [6], mixed-effect modeling of scalar measurements [8] or registration of 3D image data along time [7]. Yet, none of these model the time-change of image data represented as a function parametrized by local image properties. We aim to fill this gap through our proposed framework and demonstrate its application to DT-MRI data along white matter tracts for characterization of early neurodevelopment.

The motivation behind using DTI stems from its ability to capture microscopic tissue structure and brain connectivity noninvasively, by quantifying directional diffusion of water molecules. Changes in white matter provide an assessment of brain maturation and have been found to be correlated with functional, cognitive and behavioral developments in humans [4]. By definition, white matter tracts are attributed to characteristic cognitive functions making them pertinent in neurodevelopmental diseases where distinct cognitive deficits may be observed. Although conventional region-based DTI studies exist, white matter tract-based longitudinal analysis are rare despite being more accurate and clinically relevant [4, 9].

Our driving application is the study of infant neurodevelopment. In view of the rapid growth that marks the initial years of neurodevelopment, characterization of growth trajectories in infants is crucial for an early diagnosis of neurodevelopmental disorders [4, 2]. As an example, for disorders with a delayed onset of symptoms or in cohorts at high-risk for certain diseases, delineation of normative trends and any individual deviations from these may indicate developmental abnormalities where an early therapeutic intervention may have the potential to alter or even reverse disease progression [5].

This paper presents a new framework for temporal modeling of a set of discrete functions which are longitudinal in design. The methodology estimates patient-specific, spatiotemporal trajectories and computes a normative trajectory using individual trends. In this process, a template baseline curve is also estimated which provides an unbiased initialization to the temporal trend. Section 2 details the framework along with mathematical derivations. Section 3 includes validation using synthetic data and results of application to pediatric DTI data.

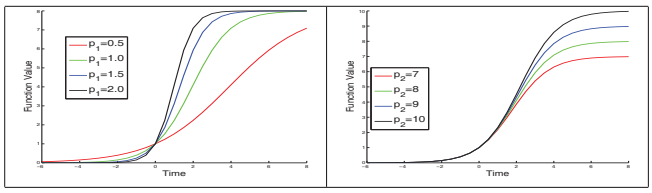
2. METHOD

2.1. Framework

As a general representation, let $g_{t_k}(s)$ be a function parametrized by an independent spatial variable s, representing information for an

*Supported by NIH grants National Alliance for Medical Image Computing (NA-MIC) U54 EB005149, R01 HD055741, R01 MH070890, Conte Center MH064065, and BRP R01 NS055754.

Fig. 1. Effect of varying p_1 and p_2 on a 1D logistic curve.



individual subject at timepoint t_k with N_c number of longitudinal timepoint curves such that $k = [1 \cdots N_c]$. To model the spatiotemporal trajectory, let a spline curve $f_t(s)$ estimate g, at time t and spatial location s (assuming g and f are continuous along s and t). We parametrize $f_t(s)$ by a set of N control points with time-varying weights $\alpha_i(t)$ spatially defined at locations s_i along s. For a continuous formulation, we use a non-parametric kernel smoother along s to estimate $f_t(s)$ from discrete weights $\alpha_i(t)$ at s_i, allowing the functions to represent any spatially continuous information in the absence of known priors and constraints. For capturing temporal behavior, we employ a parametric approach to model the dynamics of spline curve $f_t(s)$ via the evolution of weights $\alpha_i(t)$ associated with the control points. This provides a compact description of the overall trajectory based on the number of model parameters and locations s_i. Given the inherent correlation between the dynamics of points induced by the smoothing kernel, we sample the control points at every kernel's width σ along arc-length where σ provides the trade-off between data fidelity and overfitting. For longitudinal DTI changes along white matter tracts in infants, $g_{t_k}(s)$ represents scalar invariants derived from diffusion tensors (like FA) as g, parametrized by the gestational age t_k and the arc length s along tract's length L. Goodlett et al. provide more details on this representation along with the spatial normalization achieved across subjects by a consistent arc length parametrization of the tract geometry [10].

We now formulate the goodness-of-fit criterion and system constraints in equations (1) to (4) in the context of our driving application assuming a Gaussian noise distribution. We use a Gaussian kernel $G(.)$ along s, with standard deviation σ and $\alpha_i(t)$ as the dependent variable, to capture along-tract correlation in the diffusion data expected due to the underlying brain anatomy. The temporal modeling for all i, is done using the Verhulst-Pearl logistic function parametrized by the rate of growth defined per unit time and weight (p_{1i}), the carrying capacity (p_{2i}) and the initial condition at t=0 (α_{0i}). The logistic evolution is nearly exponential when the current function value is low. As it increases, the carrying capacity limits the rate of function change till the function saturates to the value of the asymptote (same as the carrying capacity). This behavior mimics diffusion changes observed in neonatal brain where the change is driven by the current diffusion value. For increasing trends like that of Fractional Anisotropy, we observe accelerated changes in FA during early brain maturation which slow down considerably with time as FA increases[10]. Intuitively, p_1 tells us how fast the function grows towards the saturation value of the asymptote p_2, given the initial value α_0 at t=0 (Fig 1) where $\alpha_0(s)$ is the template function curve providing an unbiased baseline estimate at t=0.

2.2. Mathematical formulation

$$E(\alpha_0, p_1, p_2) = \Sigma_{k=1}^{N_c} \int_0^L (f_{t_k}(s) - g_{t_k}(s))^2 ds \tag{1}$$

such that,

$$f_t(s) = \Sigma_{i=1}^{N} G_\sigma(s - s_i) * \alpha_i(t) \tag{2}$$

$$\dot{\alpha}_i(t) = p_{1i} * \alpha_i(t) * (1 - \frac{\alpha_i(t)}{p_{2i}}) \tag{3}$$

$$\alpha_i(0) = \alpha_{0i}. \tag{4}$$

Given equations (1) and (2), the gradient of the criterion is

$$\begin{aligned} \nabla_{\mathbf{p_i}} E &= 2 * \Sigma_{k=1}^{N_c} (\int_0^L G(s - s_i) * (f_{t_k}(s) - g_{t_k}(s)) ds) \\ &\quad \cdot \nabla_{\mathbf{p_i}} \alpha_i(t_k) \\ \nabla_{\alpha_{0i}} E &= 2 * \Sigma_{k=1}^{N_c} (\int_0^L G(s - s_i) * (f_{t_k}(s) - g_{t_k}(s)) ds) \\ &\quad \cdot \nabla_{\alpha_{0i}} \alpha_i(t_k) \end{aligned} \tag{5}$$

which for all i, requires computing the variation of the whole path $\alpha_i(t)$ when the parameters α_{0i}, p_{1i} and p_{2i} are varied. For this purpose, we rewrite $\alpha_i(t)$ from (3) and (4) as a function F of its independent variables, with $\mathbf{p_i}$ as a 2×1 vector containing $[p_{1i}\ p_{2i}]^T$,

$$\frac{d}{dt}\alpha_i(t) = F(\alpha_i(t), \mathbf{p_i})\ ; \alpha_i(0) = \alpha_{0i}.$$

We now apply calculus of variations. A small perturbation in the independent variables $\delta\mathbf{p_i}$ and $\delta\alpha_{0i}$ introduces perturbations in the intermediate dependent variable $\delta\alpha_i(t)$, which satisfy the linearized ODE:

$$\begin{cases} \frac{d}{dt}(\delta\alpha_i(t)) = \partial_\alpha F * \delta\alpha_i(t) + \nabla_{\mathbf{p}} F^T \cdot \delta\mathbf{p_i} \\ \delta\alpha_i(0) = \delta\alpha_{0i} \end{cases} \tag{6}$$

Eq (6) is a linear, non-homogeneous ODE, the generic solution of which is

$$\delta\alpha_i(t) = R_{0t} * \delta\alpha_{0i} + \int_0^t R_{vt} * \nabla\mathbf{p} F(v)^T dv \cdot \delta\mathbf{p_i}$$

where R_{st} is defined as $\exp(\int_s^t \partial_\alpha F(\alpha_i(u), \mathbf{p_i}) du)$ for all s and t. This shows that

$$\nabla_{\mathbf{p_i}} \alpha_i(t) = \int_0^t R_{vt} * \frac{d}{d\mathbf{p}} F(v)^T dv, \tag{7}$$

$$\nabla_{\alpha_{0i}} \alpha_i(t) = \exp\left(\int_0^t \frac{d}{d\alpha} F(\alpha_i(u), \mathbf{p_i}) du \right). \tag{8}$$

For (7), one notices that $R_{ut} = \mathrm{id} + \int_u^t \partial_\alpha F(s) R_{us} ds$, which gives using Fubini's theorem

$$\nabla_{\mathbf{p_i}} \alpha_i(t) = \int_0^t \nabla_{\mathbf{p}} F(u) + d_\alpha F(u) * \nabla_{\mathbf{p_i}} \alpha_i(t)\ du.$$

Thus, the gradient can be computed by solving a linear ODE:

$$\begin{cases} \frac{d}{dt} \nabla_{\mathbf{p_i}} \alpha_i(t) = \nabla_{\mathbf{p}} F(t) + d_\alpha F(t) * \nabla_{\mathbf{p_i}} \alpha_i(t), \\ \nabla_{\mathbf{p_i}} \alpha_i(0) = [0, 0]^T. \end{cases} \tag{9}$$

Equation (8) shows that $\nabla_{\alpha_{0i}} \alpha_i(t)$ can be also solved via forward integration of ODE:

$$\begin{cases} \frac{d}{dt} R_{0t} = d_\alpha F(t) * R_{0t} \\ R_{00} = 1 \end{cases} \tag{10}$$

where R_{0t} is equal to $\nabla_{\alpha_{0i}} \alpha_i(t)$ for all t. Plugging (9) and (10) in the gradient of E (5) completes the formulation.

2.3. Implementation

We implement a gradient descent scheme to minimize E and fit the model to $g_{t_k}(s)$ by optimizing α_{0i} and $\mathbf{p_i}$ based on eq (5) using gradient descent step sizes $(\eta_{\alpha_0}, \eta_{\mathbf{p}})$ respectively. Even though the change in one parameter $(p_1(s))$ is calculated independently of the other two parameters $(p_2(s), \alpha_0(s))$, E is jointly minimized by simultaneously updating all parameters in each iteration. $\forall i$,

$$\mathbf{p_i}^{new} = \mathbf{p_i} - \eta_{\mathbf{p}} * (\nabla_{\mathbf{p_i}} E) \; ; \; \alpha_{0i}^{new} = \alpha_{0i} - \eta_{\alpha_0} * (\nabla_{\alpha_{0i}} E).$$

2.4. Extension to multiple subjects

We extend the above framework to simultaneously estimate individual trends for multiple subjects while allowing inter-subject comparison. We create a common reference frame by assuming that all subjects start the 'same' with a common template function $\alpha_0(s)$ estimated globally, along with individualized per unit growth rate $p_1^B(s)$ and asymptote $p_2^B(s)$, given N_B number of subjects with superscript B implying individual information. The new criterion is given by,

$$\begin{aligned} E_{total}(\alpha_0, \mathbf{p}^B) &= \Sigma_{B=1}^{N_B}(\Sigma_{k=1}^{N_c} \int_0^L (f_{t_k}^B(s) - g_{t_k}^B(s))^2 ds) \\ &= \Sigma_{B=1}^{N_B}(E^B(\alpha(0), \mathbf{p}^B)) \end{aligned}$$

such that,

$$\begin{aligned} f_t^B(s) &= \Sigma_{i=1}^{N} G(s - s_i) * \alpha_i^B(t), \\ \dot{\alpha}_i^B(t) &= p_{1i}^B * \alpha_i^B(t) * (1 - \frac{\alpha_i^B(t)}{p_{2i}^B}), \\ \alpha_i^B(0) &= \alpha_{0i}. \end{aligned}$$

Accordingly, the gradient of the criterion is modified.

$$\nabla_{\mathbf{p_i^B}} E_{total} = \nabla_{\mathbf{p_i^B}} E^B \; ; \; \nabla_{\alpha_{0i}} E_{total} = \Sigma_{B=1}^{N_B}(\nabla_{\alpha_{0i}} E^B).$$

3. EXPERIMENTS

Representing the change trajectory with a small set of descriptive parameters is one of key strengths of this framework. Second, being parametrized, the model addresses challenges arising from the timing of acquiring DTI scans—key timepoints missing, irregular time spacing and lack of time correspondence across subjects. Third, a continuous evolution is inferred by matching all available timepoint curves simultaneously, thus utilizing global information for estimation. Fourth, since the template curve is also estimated by the model, the temporal growth is unbiased by the shape of any fixed baseline curve or individual $g_{t_k}(s)$ functions. The local dynamics of an individual point along arc-length is monotonic due to the logistic growth model. The value may be either increasing (or decreasing) depending on if p_2 is greater (or lesser) than α_0.

3.1. Validation using synthetic data

We validate the framework with synthetic $g_{t_k}(s)$ for 4 subjects with 3 timepoints, generated with known values of $p_1^B(s) = (1.3, 1.4, 1.5, 1.6)$, $p_2^B(s) = (0.5, 0.7, 0.9, 1.1)$ respectively for each B, $\forall$ s and a common $\alpha_0(s)$ curve. We experiment with two different levels of Gaussian noise added to $g_{t_k}(s)$, variance ($\sigma^2 =$) 0.01 and 0.05. We initialize the model parameters with random constant values for (p_1, p_2, α_0) $\forall$ s and kernel width $\sigma = 4$ and 6 respectively. This downsampling avoids overfitting as well as captures the trend with much lower number of parameters leading to strong data reduction. Estimated $f_{t_k}(s), (p_1(s), p_2(s), \alpha_0(s))$ are shown in Fig 2 and RMSE as a measure of residual error is provided in Table 1. Despite the noise, large variability in the true trajectories across subjects and a downsampling to less than 25% spatial locations, the recovered information seems to be in agreement with the true values.

Fig. 2. Synthetic data validation: Left: $\sigma^2 = 0.01$, Right: $\sigma^2 = 0.05$. 1st row: $g_{t_k}^B(s)$ (red), $f_{t_k}^B(s)$ (blue), $f_t^B(s)$ (green), $\alpha_0(s)$ (black), 2nd row: Noisy (magenta) and Estimated (blue) curves in 2D , 3rd row: true (solid) versus estimated (circles) model parameters $(p_1(s), p_2(s), \alpha_0(s))$ for 4 subjects (red,green,blue,magenta)

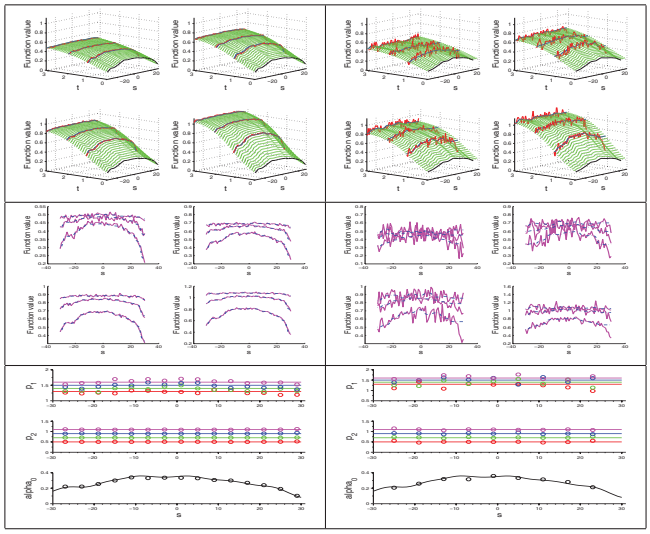


Table 1. RMSE for synthetic data validation results (Fig 2)

noise variance (σ^2)	$f_t(s)$	$\alpha_0(s)$	$p_1(s)$	$p_2(s)$
0.01	0.0109	0.0115	0.0671	0.0091
0.05	0.0558	0.0203	0.1294	0.0269

3.2. Application to pediatric data

We apply our method to pediatric longitudinal DTI data (FA curves for the genu tract) from 15 infants, scanned at approximately 2 weeks, 1 year and 2 year (scan times are not in perfect correspondence). Naturally, brain growth starts with gestation but we do not yet have reliable estimates of tract-specific diffusion from in-utero imaging [4]. We therefore make the assumption that subjects share a common template diffusion profile $\alpha_0(s)$ at gestational age approximately 0. Results with $\sigma = 4$ are summarized in Fig 3. Next, we utilize the fine, consistent sampling along t and s across estimated individual trajectories to compute average and standard deviation at every available (t, s) pair, generating a normative growth model which summarizes natural brain maturation variability (Fig 4). Fitting our growth model to the normative spatiotemporal trajectory gives back estimated $(p_1(s), p_2(s), \alpha_0(s))$ quantifying the normative growth (Fig 5). We visualize these normative model parameters by mapping them back to the original coordinate space of the 3-D genu tract to allow anatomically relevant interpretations (Fig 5). The

Fig. 3. Application to pediatric data (15 subjects, 3 timepoints): Left: Estimated trajectories for 4 of the 15 subjects (refer to Fig 2 for color codes). Right: Estimated $(p_1^B(s), p_2^B(s), \alpha_0(s))$

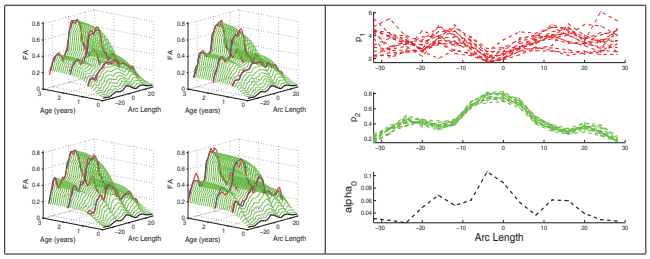
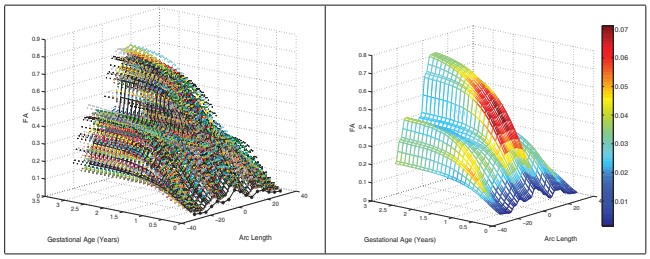


Fig. 4. Normative trajectory: Left: Individual (dots) versus normative (black lines) trajectory. Right: Normative trajectory colored by population standard deviation.

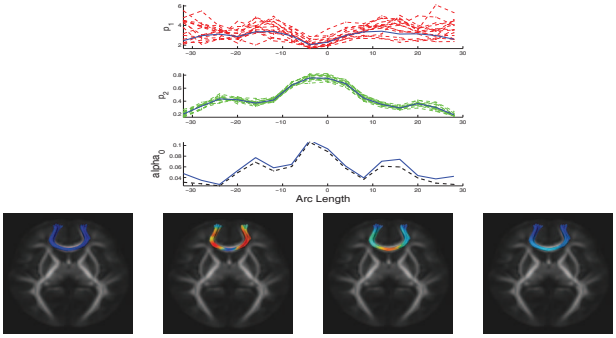


results point to interesting observations like individuals saturate to almost similar asymptote values by the end of the third gestational year given by the low variability in $p_2^B(s)$ (Fig 3). Maximum variability across individuals is observed around gestational age of 1.5 years with differences already present around birth (approximate gestational age of 0.75 years) and localized temporal trends are seen along the length of the tract (Fig 4). Fig 5 (bottom row) shows that normative $\alpha_0(s)$ and normative $f_t(s)$ at-birth indicate low FA values with some degree of diffusion anisotropy already present around birth. Normative $p_2(s)$ shows a high degree of anisotropy specially in the middle of the tract by gestational age 3. Red regions along normative $p_1(s)$ represent locations where FA maturates rapidly to reach $p_2(s)$ while the blue regions show a relatively delayed maturation along time. These results provide a proof of concept for the proposed methodology and its potential application to large clinical studies for a reliable assessment of growth functions for individuals and populations.

4. CONCLUSION

We present a novel methodology that takes a set of discrete functions over time which are spatially in correspondence, and fits a growth model via the template curve to capture their temporal change with a small number of descriptive parameters. The framework quantifies individual trends and group statistics of growth parameters which may answer clinical questions related to delayed or accelerated growth of individuals and populations, and is designed to answer questions such as if individuals would eventually rejoin average trajectories. Future work will include statistical models and hypotheses testing schemes based on these growth parameters and regression manifolds, for comparing normative data with individuals or groups with application to large clinical studies.

Fig. 5. Top: Estimated normative model parameters (blue) versus individual parameters. Bottom: Estimated normative parameters visualized in the coordinate space of genu tract. Left to right: $(\alpha_0(s), p_1(s), p_2(s), f_t(s)$ at-birth). Color scale is red (high) to blue (low).



5. REFERENCES

[1] B. Davis, P.T. Fletcher, E. Bullitt, and S. Joshi, "Population shape regression from random design data," in *Proc. of ICCV '07*, 2007, pp. 1–7.

[2] M. Kuklisova-Murgasova, P. Aljabar, and D. Rueckert et al., "A dynamic 4d probabilistic atlas of the developing brain," *NeuroImage*, vol. 54, no. 4, pp. 2750 – 2763, 2011.

[3] K. Pohl, J. Fisher, M. Shenton, R. McCarley, W. Grimson, R. Kikinis, and W. Wells, "Logarithm odds maps for shape representation," in *MICCAI 2006*, vol. 4191 of *Lecture Notes in Computer Science*, pp. 955–963. 2006.

[4] J. Dubois, L. Hertz-Pannier, and D. Le Bihan et al., "Assessment of the early organization and maturation of infants' cerebral white matter fiber bundles: A feasibility study using quantitative diffusion tensor imaging and tractography," *NeuroImage*, vol. 30, no. 4, pp. 1121 – 1132, 2006.

[5] National Advisory Mental Health Council, "Transformative neurodevelopmental research in mental illness," Tech. Rep., National Institute of Mental Health, 2011.

[6] H. Tiemeier, R. K. Lenroot, D. K. Greenstein, L. Tran, R. Pierson, and J. N. Giedd, "Cerebellum development during childhood and adolescence: A longitudinal morphometric mri study," *NeuroImage*, vol. 49, no. 1, pp. 63 – 70, 2010.

[7] A. D. Leow, A. D. Klunder, and P. M. Thompson et al., "Longitudinal stability of mri for mapping brain change using tensor-based morphometry," *NeuroImage*, vol. 31, no. 2, pp. 627 – 640, 2006.

[8] S. Xu, M. Styner, and G. Gerig, "Multivariate nonlinear mixed model to analyze longitudinal image data: Mri study of early brain development," *Proc. of IEEE workshop on MMBIA*, June, 2008.

[9] H. Zhu, M. Styner, N. Tang, Z. Liu, W. Lin, and J.H. Gilmore, "Frats: Functional regression analysis of dti tract statistics," *Medical Imaging, IEEE Transactions on*, vol. 29, no. 4, pp. 1039 –1049, april 2010.

[10] C. Goodlett, P.T. Fletcher, J.H. Gilmore, and G. Gerig, "Group analysis of dti fiber tract statistics with application to neurodevelopment," *Neuroimage*, vol. 45, no. 1 (suppl 1), pp. S133–S142, 2009.